# Evolution of Precipitate Microstructure During Creep of an AA7449 T7651 Aluminum Alloy

G. FRIBOURG, Y. BRÉCHET, J.L. CHEMIN, and A. DESCHAMPS

Creep forming is a process where plastic deformation is applied at the material's aging temperature. It enables to obtain parts of complex shape with reduced internal stresses and finds applications, for instance, in the aerospace industry. In this article, we report *in-situ* small-angle X-ray scattering measurements during creep experiments carried out on an AA7449 Al-Zn-Mg-Cu alloy in the T7651 temper. In the range of temperatures of 413 K to 453 K (140 °C to 180 °C), we show that the initial microstructure is not stable with respect to the applied stress/strain. Accelerated precipitation coarsening is shown to occur, clearly related to the plastic deformation. This strain-induced microstructure evolution is shown to happen even at temperatures well below the aging temperature that has led to the initial temper.

DOI: 10.1007/s11661-011-0786-9


## I. INTRODUCTION

ALUMINUM alloys of the Al-Zn-Mg-Cu series are among the major materials for aerospace applications.[1] Their classical process route for modern airplane structures involves a heat treatment carried out on thick plates or forgings, followed by machining to the desired shape. The quench step from the solution treatment temperature, carried out on plates of large dimensions, results in high levels of internal stresses due to through thickness temperature gradients and heterogeneous plastic flow during quenching. These internal stresses are only partially removed by stress-relieving plastic deformation carried out prior to the aging treatment.[2] They can result in part distortion after machining and reduced fatigue resistance.

An alternative process route is creep forming, where the material is loaded elastically and subsequently heated to the heat treatment temperature, therefore deforming plastically to the desired shape.[3] Creep forming has the advantage of reducing the level of internal stress due to the reduced flow stress at the aging temperature and allowing for the forming of complex shapes (*e.g.*, with double curvature) with reduced springback effect. Creep forming of precipitation hardening aluminum alloy has received some attention in the literature, mainly from the structural mechanics point of view, where authors aimed at providing appropriate constitutive laws to describe the deformation behavior of the material under the combination of temperature and stress (*e.g.*, References 4 and 5). However, one concern arises about the evolution of the precipitate microstructure specifically induced by the plastic deformation, and therefore about the possibility of obtaining inhomogeneous materials properties in the manufactured part due to inhomogeneous levels of experienced plastic strain. Dynamic precipitation under plastic strain in the aluminum alloy is a relatively well-chartered area;[6–8] however, several phenomena can occur depending on the combination of the initial state of the material (supersaturated solid solution or containing precipitates), temperature, and strain rate. Precipitation can be enhanced by plastic strain or, alternatively, precipitates can be dissolved. The microstructure evolution during creep forming has received sparse attention in the literature.[9–13] In 7000 series aluminum alloy, Li *et al.*[14] very recently showed some accelerated precipitate growth and coarsening that led to a reduction of mechanical properties. However, a quantitative analysis of the evolution of precipitates as a function of temperature and applied creep stress is not available yet.

The aim of this article is to provide a quantitative evaluation of the extent of the evolution of precipitate microstructures during creep deformation on the classical aerospace alloy AA7449 initially in the T7651 temper. This will be achieved by using *in-situ* small-angle X-ray scattering during load-control tensile tests. The mechanical testing will be carried out both above the temperature at which the T7651 microstructure was obtained [namely, 433 K (160 °C)] and below, in order to evaluate the temperature range where significant precipitate evolution can be expected to occur. Due to the fact that these experiments were carried out using a synchrotron X-ray source, the beam time was limited and the creep experiments, therefore, will be limited to relatively short times, yet consistent with processes such as creep forming.

G. FRIBOURG, formerly PhD Student, Grenoble Institute of Technology, Grenoble, France, is now a Research Engineer, SNECMA, Gennevilliers, 92702 Colombes, France. Y. BRÉCHET and A. DESCHAMPS, Professors, and J.L. CHEMIN, Research Engineer, are with the SIMAP Laboratory, INP Grenoble-NRS-UJF, 38402 St Martin d'Hères Cedex, France. Contact e-mail: alexis.deschamps@grenoble-inp.fr

Manuscript submitted December 6, 2010.
Article published online July 20, 2011

## II. MATERIALS AND METHODS

### A. *Alloy and Experimental Procedure*

The studied material is an AA7449 alloy, a wrought aluminum alloy of the Al-Zn-Mg-(Cu) family. The specific composition of the received plate, provided by Alcan–Centre de Recherches de Voreppe (France), was 8.3 wt pct zinc, 2.2 wt pct magnesium, and 1.9 wt pct copper. The as-received temper was T7651, *i.e.*, pre-strained and overaged. The industrial aging treatment consists of a water quench from the solution treatment temperature, a plastic deformation of about 2 pct, a few days of natural aging, and a two-step aging treatment: 6 hours at 393 K (120 °C) and 10 hours at 433 K (160 °C).

Small-angle scattering experiments were carried out at the European Synchrotron Research Facility (ESRF) on the BM02/D2AM beamline, at a wavelength of 1.3 Å. The accessible range of scattering vectors was [0.007, 0.4] $Å^{-1}$, and the beam diameter was 200 $\mu$m. CCD camera data were corrected for read-out noise, distortion, flat field, and background noise. They were normalized using a reference sample and transmission measurements through calibrated filters. The experiments were carried out with a specially designed tensile heating rig, allowing for *in-situ* SAXS measurements in transmission through the sample during the tensile tests, which were described in Reference 15. The tensile samples had a thickness of 150 ± 2 $\mu$m and a gage length of 4 mm. The two crossheads moved symmetrically in order to ensure that the area covered by the X-ray beam (located in the middle of the gage length) remained the same during the entire tensile test. The deformation was measured by an LVDT sensor.

### B. *Characterization of the Initial Microstructure*

Figures 1(a) and (b) show a transmission electron microscopy bright-field micrograph and a diffraction pattern of the initial temper. Following the analysis of the $\{111\}_{Al}$ diffraction patterns of Reference 16, the microstructure corresponds to a dense distribution of

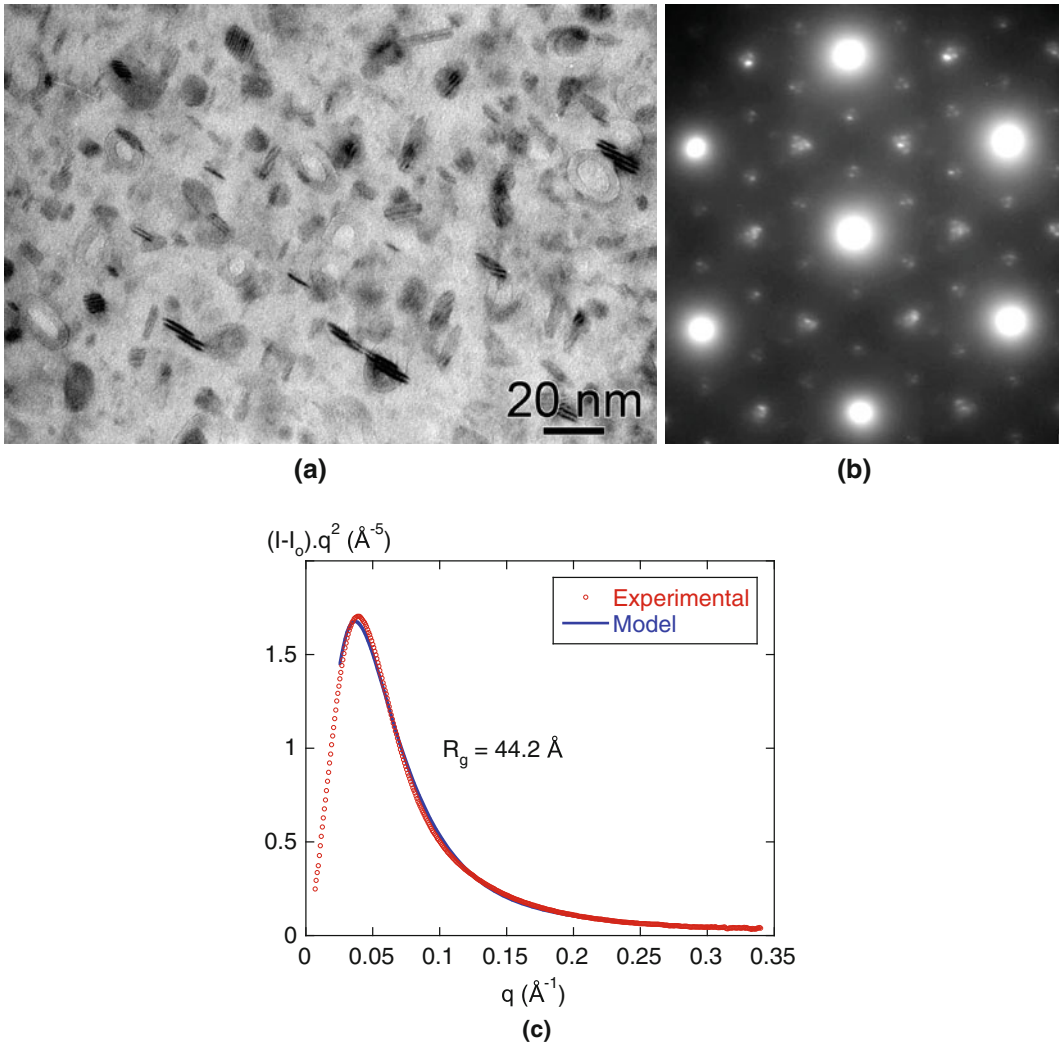


Fig. 1—Characterization of the AA7449 T7651 initial state. (*a*) Bright-field TEM micrograph (close to a $\langle 110 \rangle_{Al}$ zone axis). (*b*) TEM diffraction pattern ($\langle 111 \rangle_{Al}$ zone axis). (*c*) SAXS curve in the Kratky representation $I{\cdot}q^2$ *vs* $q$.

mostly equilibrium $\eta$ particles. The corresponding SAXS curve is shown in Figure 1(c) in a Kratky representation. The precipitate volume fraction was calculated using the integral intensity of the SAXS signal with appropriate extrapolations outside the measured range of scattering vectors, and the same composition hypothesis for the precipitates as in Reference 17, leading to a volume fraction of 6 pct. The precipitate size was calculated from the Guinier approximation using the self-consistent procedure described in Reference 18, where it was shown that this method provided an accurate measurement of the precipitate size in the case of a polydisperse distribution of precipitates with moderate aspect ratio. The reproducibility of the measured precipitate radii and volume fractions in the different samples tested was approximately ±0.1 nm and ±0.1 pct. One should note that, additionally, smaller relative variations can be detected during *in-situ* tests, so that accurate measurements of the precipitate growth rate can be achieved.

### C. *Description of the Testing Procedure*

Creep tests were carried out in the following way. First, the temperature of the sample was raised to the desired value, and allowed to homogenize along the sample gage length. The temperature increase lasted approximately 1 minute, and the total duration of this stage was 2 minutes, during which the sample was kept in load control under a constant stress of about 20 MPa to allow for thermal dilatation of the system. Then, the test was started in displacement control until the yield stress was reached, in order to obtain an accurate value of the yield stress of each sample individually. This stage lasted for 1 minute. Thereafter, the system was changed to load control again, and a prescribed fraction of the measured yield stress was applied, while recording the sample deformation. During most tests, several loads were applied sequentially to evaluate the effect of creep stress on creep strain. Reported creep strain rates will be steady-state values. In all cases, tests in the same condition were carried out without an applied load to evaluate precisely the effect of plastic strain on the microstructure evolution.

### D. *Creep Rates*

In this section, we report the creep strain rates experienced by the material in the investigated range of temperatures and creep stresses. The microstructure evolutions corresponding to these conditions will be presented in Sections IV and V.

Figure 2 shows first the evolution of the alloy's yield stress with temperature, from room temperature up to 463 K (190 °C). It was checked on room temperature samples that the yield stress measured on the small samples with the *in-situ* tensile rig corresponded to that measured on macroscopic samples. A continuous decrease is observed that becomes really significant at temperatures above 413 K (140 °C).

Figure 3(a) shows the steady-state creep rates as a function of creep stress for all the investigated temperatures.

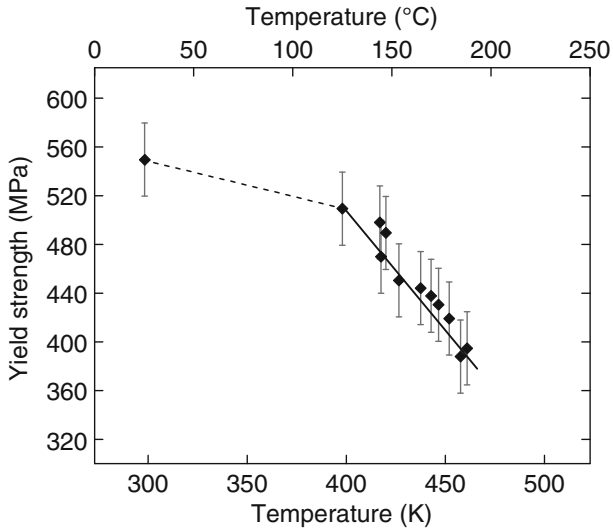


Fig. 2—Yield stress as a function of temperature measured on the initial temper of the material at a strain rate of $10^{-4}$ $s^{-1}$.

In Figure 3(b), the same data are shown as a function of the ratio between the creep stress and the yield stress (reduced stress) at the testing temperature. A rapid increase of strain rate is observed with increasing creep stress, and of course the stress required to obtain a given value of strain rate decreases with increasing temperature, as shown in Figure 3(b).

## III. MICROSTRUCTURE EVOLUTION AT 180 °C

In this section, we will present the microstructure evolution that occurs during creep tests carried out at temperatures above the aging temperature of the T7651 initial state [namely, 433 K (160 °C)]. It is expected that the microstructure evolution at such high temperatures is rapid, even in the absence of applied stress. Therefore, it is particularly important in this case to evaluate the difference between the microstructure evolution with and without applied stress.

Figure 4 shows the evolution of (a) precipitate radius and (b) volume fraction during the tensile test at 453 K (180 °C). During the heating stage and the loading stage to the material's yield point, a significant evolution of precipitates occurs, in accordance with the relatively high temperature investigated here. The precipitate volume fraction is observed to decrease from 6 to about 5 pct, and subsequently remains stable. This value should be close to the equilibrium volume fraction (corrected by the Gibbs–Thomson effect) at this temperature. Because the behavior of volume fraction is similar for all the other temperatures, it will not be presented in the forthcoming experiments. The precipitate radius increases during this stage by about 2 Å.

During the creep stage, a rapid evolution of precipitate size is observed in the material experiencing a stress of 375 MPa as compared to the unstressed specimen. A precipitate evolution in the sample stressed at 206 MPa is also observed, yet much smaller.

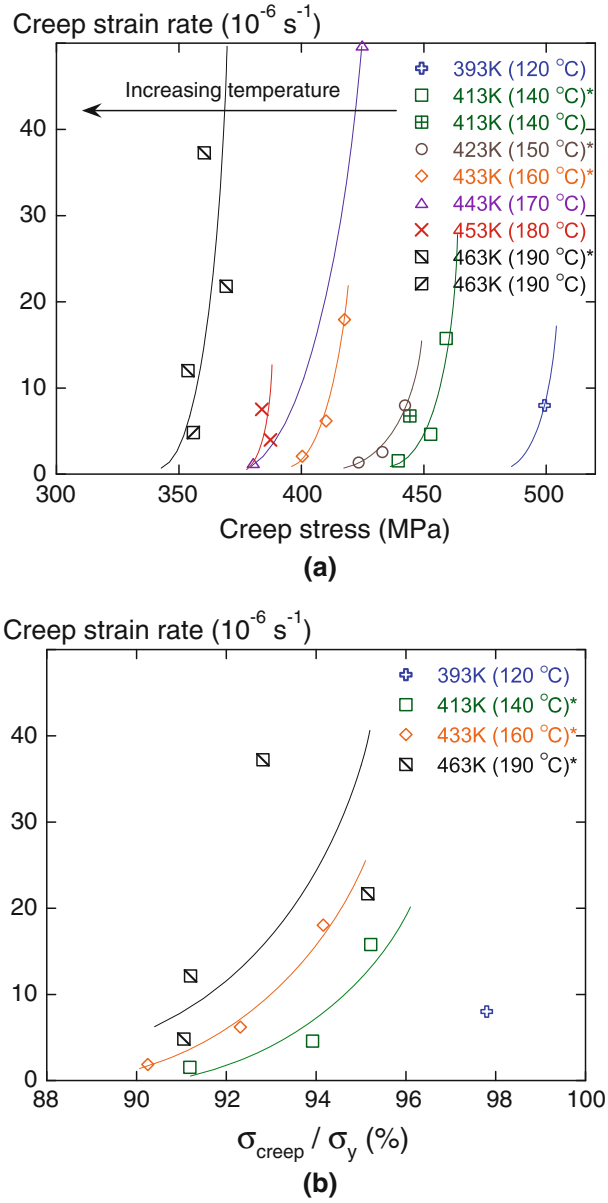


Fig. 3—(*a*) Steady-state creep rate as a function of applied stress for the different tested temperatures. (*b*) Same data represented as a function of the ratio between the applied stress and the yield stress at the testing temperature. The stars correspond to data points obtained on a single sample where the applied stress was changed during the tensile test. The lines are not fits to the experimental data points but simply guidelines to help in visualizing the data.

Figure 4(c) shows the evolution of strain in the sample stressed at 375 MPa together with the radius evolution rate $dR/dt$, both for the stressed and unstressed specimens. As shown previously, in both materials, there is a sharp peak in the rate of radius evolution during the heating stage. After this transient stage, where the volume fraction adjusts to near the equilibrium value at 453 K (180 °C), the unstressed specimen shows a relatively constant radius growth rate, corresponding to precipitate coarsening. The stressed specimen shows a larger growth rate, increasing with time. This growth rate is quite clearly related to the occurrence of plastic strain that increases also in the same time range. Figure 4(d) represents the same radius growth rate, this time together with the stain rate. Although the two are also observed to increase together, the correlation seems much less obvious.

## IV. MICROSTRUCTURE EVOLUTION AT AND BELOW 160 °C

In this section, we will present the microstructure evolution during creep in the temperature range 393 K to 433 K (120 °C to 160 °C). Since the T7651 material was aged 10 hours at 433 K (160 °C), the evolution of precipitates during 20 minutes at 433 K (160 °C) or below without an applied stress is negligible, and will therefore not be presented here.

Figure 5 shows the microstructure evolution at 433 K (160 °C). During the entire tensile test, the precipitate size is observed to increase from 45 to 50 Å. In this case, several levels of stress were applied during the same test. It is apparent in the strain evolution that the strain rate increases together with the applied stress. The radius growth rate appears to follow the same behavior, and again correlates well with the strain evolution.

Figure 6 shows similar results obtained at 423 K (140 °C), where the precipitate microstructure evolution in the absence of strain is negligible (20 K below the temperature of the initial heat treatment). During this test, the evolution of precipitates has a much more limited extent, as expected from the lower temperature. However, it is still significant, namely, an increased size of more than 2 Å during the test, despite a temperature 20 K below the aging temperature of the alloy. As for the previous case, the applied load was varied during the test, resulting in an acceleration of the strain rate. However, this time the correlation between the strain and precipitate growth rate is not obvious. This may be related to the very low precipitate growth rate experienced here.

## V. DISCUSSION AND CONCLUSIONS

The combination of the precision of the precipitate size measurements by the SAXS technique and the *in-situ* nature of the experiments reported here enables improvement of the understanding of the microstructure evolution during creep deformation of materials containing precipitates. In particular, we showed that plastic deformation applied at the aging temperature induces an accelerated precipitate coarsening that we have quantified through the precipitate growth rate. This acceleration of precipitate coarsening is, as expected, more important as the temperature or the applied stress is raised. It can happen at temperatures well below the aging temperature of the alloy, which was 433 K (160 °C) for the AA7449 T7651 material.

Several mechanisms can account for an accelerated coarsening of precipitates under plastic strain. The introduction of dislocations within the material can increase the apparent diffusion rate by promoting pipe diffusion along the dislocation lines. However, some

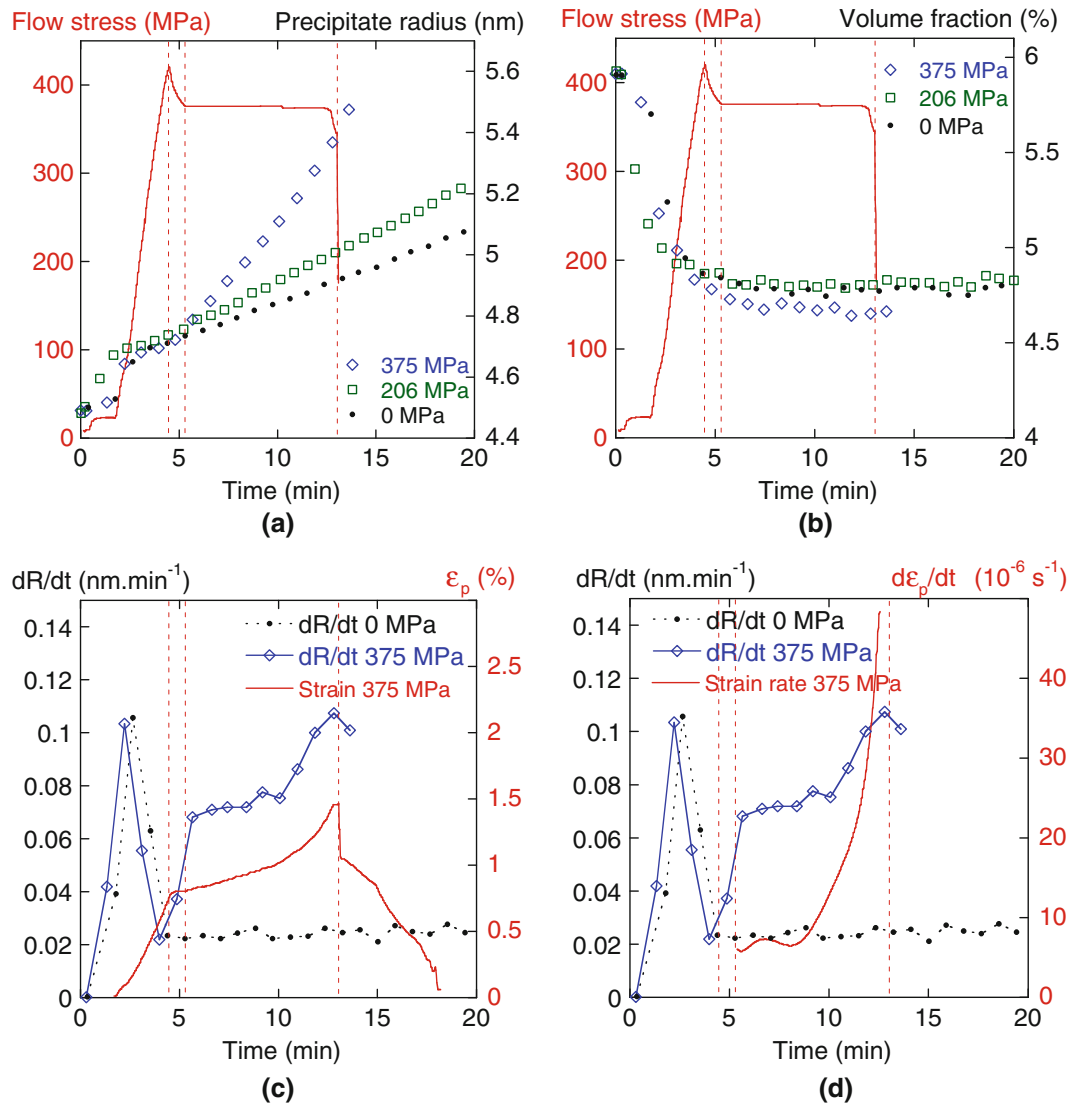


Fig. 4—Evolution of microstructure and strain during testing at 453 K (180 °C). (*a*) Evolution of precipitate size (and applied stress for the 375 MPa test) with time in the unstressed specimen and for an applied stress of 206 or 375 MPa. (*b*) Evolution of volume fraction in the same conditions. (*c*) Evolution of the precipitate growth rate and strain. (*d*) Evolution of the precipitate growth rate and strain rate.

dislocations were already present in the initial state since the material was stress relieved before aging to the T7651 temper. Thus, it seems unlikely that a few percent extra plastic deformation would, by itself, increase the precipitate coarsening rate by orders of magnitude, as was observed here, especially at low temperatures. Therefore, the movement itself of the dislocations, and not only their presence, has to play a key role in the microstructure evolution. However, it does not seem possible here to invoke a "solute collector" mechanism for the sweeping dislocations, since the material is initially in an overaged state, so that the matrix is already solute depleted. No increase in volume fraction was actually observed during the tensile tests, meaning that the microstructure evolution is mainly caused by solute exchange between precipitates.

During their movement, dislocations make links between all the obstacles that they encounter, effectively increasing the efficiency of the solute transfer from the smallest precipitates to the largest ones. This increased efficiency of the fast diffusion path provided by dislocations between precipitates has to play a key role in the present situation. It should be quantified by an appropriate model, which is beyond the scope of this article.

Finally, this work calls for some practical consequences in the area of creep forming. We have shown that applying a plastic strain on a material aged to the T7651 temper resulted in significant variations of precipitate microstructures. The relative precipitate size variation of 10 pct measured in the present case translates into a classical Orowan law in a similar variation of yield strength. If the creep stresses and strains applied to a part of complex shape are heterogeneous, one can expect to obtain a material with heterogeneous properties, which need to be properly accounted for in structural design. The microstructure evolution occurring

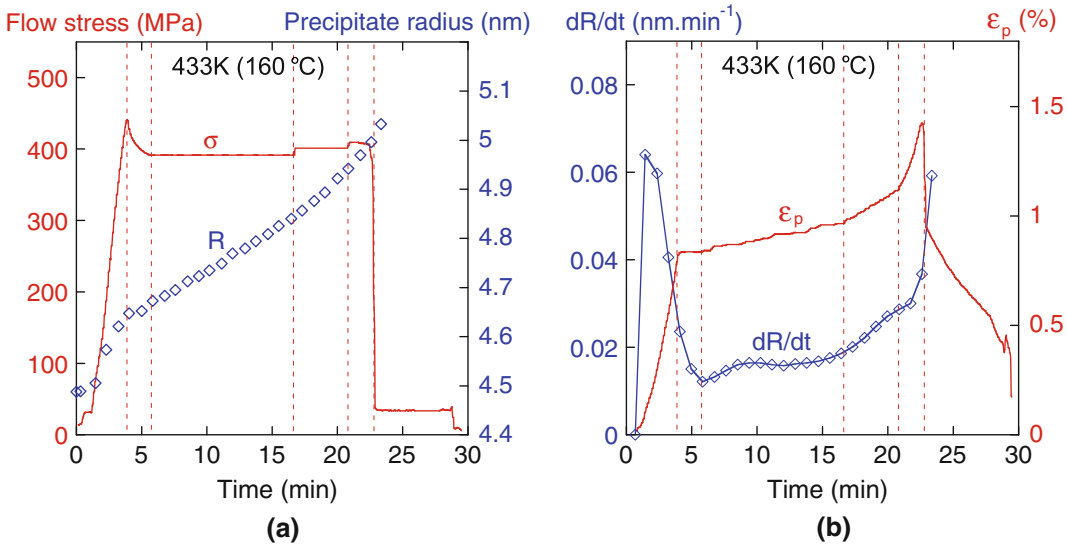


Fig. 5—Evolution of microstructure and strain during testing at 433 K (160 °C). (*a*) Evolution of precipitate size and applied stress; the vertical lines show the times for change of testing conditions. (*b*) Evolution of the precipitate growth rate and strain.

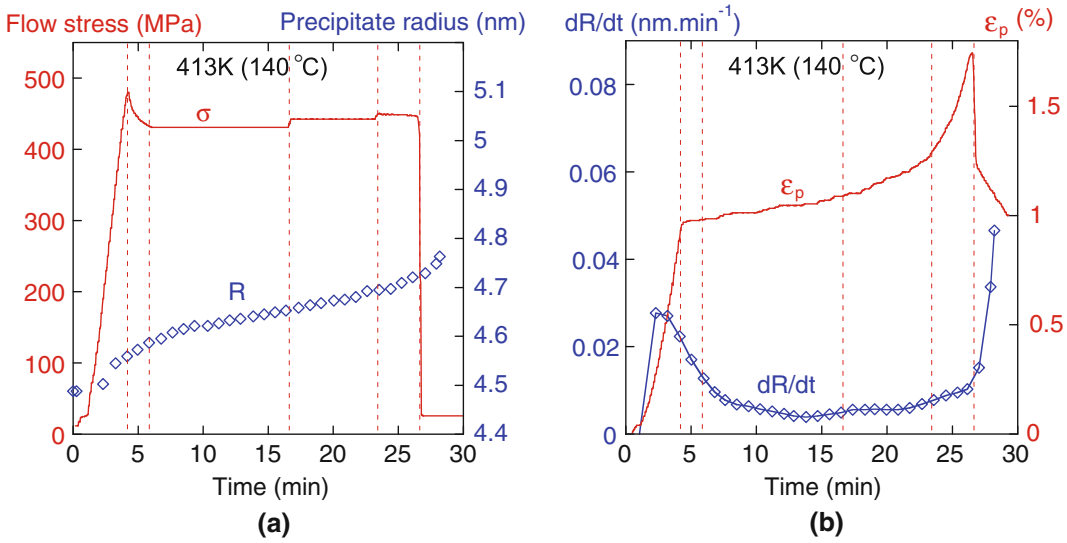


Fig. 6—Evolution of microstructure and strain during testing at 413 K (140 °C). (*a*) Evolution of precipitate size and applied stress; the vertical lines show the times for change of testing conditions. (*b*) Evolution of the precipitate growth rate and strain.

when applying plastic strain on materials with partial heat treatments was investigated as well and will be the object of a forthcoming article.

## ACKNOWLEDGMENTS

Dr. F. Bley and the staff of BM02-D2AM beamline are thanked for technical help with the experiments. This work was carried out in the COMPACT project, which is a collaboration between Airbus UK (Project Co-ordinator), Alcan–Centre de Recherches de Voreppe, Limerick University, University of Bristol, Enabling Process Technologies, University of Hannover, EADS Germany, University of Patras, Alenia Aeronautica, Ultra RS, Institut Polytechnique de Grenoble, and the University of Sheffield. The project was jointly funded by the European Union Framework 6 initiative and the project partners. Dr. U. Heckenberger is particularly thanked for fruitful discussions. One of the authors (AD) acknowledges the European Research Council for support in the framework of the NEMOLight Marie Curie International Outgoing Fellowship within the 7th European Community Framework Programme.

## REFERENCES

1. T. Warner: *Mater. Sci. Forum*, 2006, vols. 519–521, pp. 1271–78.
2. F. Heymes, B. Commet, B. DuBost, P. Lassince, P. Lequeu, and G.M. Raynaud: *1st Int. Non-Ferrous Processing and Technology Conf.*,

T. Bains and D.S. MacKenzie, eds., ASM INTERNATIONAL, Metals Park, OH, 1997, pp. 249–55.
3. M.C. Holman: *J. Mech. Work. Technol.*, 1989, vol. 20, pp. 477–88.
4. K.C. Ho, J. Lin, and T.A. Dean: *J. Mater. Proc. Technol.*, 2004, vol. 153, pp. 122–27.
5. P.P. Jeunechamps, K.C. Ho, J. Lin, J.P. Ponthot, and T.A. Dean: *Int. J. Mech. Sci.*, 2006, vol. 48, pp. 621–29.
6. A. Deschamps, F. Bley, F. Livet, D. Fabregue, and L. David: *Phil. Mag.*, 2003, vol. 83, pp. 677–92.
7. C. Genevois, D. Fabrègue, A. Deschamps, and W.J. Poole: *Mater. Sci. Eng. A*, 2006, vol. 441, pp. 39–48.
8. C.R. Hutchinson, P.T. Loo, T.J. Bastow, A.J. Hill, and J.D. Teixeira: *Acta Mater.*, 2009, vol. 57, pp. 5645–53.
9. A.W. Zhu and E.A. Starke: *J. Mater. Proc. Technol.*, 2001, vol. 117, pp. 354–58.
10. P. Cavaliere: *J. Light Met.*, 2002, vol. 2, pp. 247–52.
11. M.J. Starink, N. Gao, N. Kamp, S.C. Wang, P.D. Pitcher, and I. Sinclair: *Mater. Sci. Eng. A*, 2006, vol. 418, pp. 241–49.
12. D. Bakavos, P.B. Prangnell, B. Bes, F. Eberl, and S. Gardiner: *Mater. Sci. Forum*, 2006, vols. 519–521, pp. 407–12.
13. D. Bakavos, P.B. Prangnell, B. Bes, F. Eberl, and J.G. Grossmann: *Mater. Sci. Forum*, 2006, vols. 519–521, pp. 333–38.
14. C. Li, M. Wan, X.D. Wu, and L. Huang: *Mater. Sci. Eng. A*, 2010, vol. 527, pp. 3623–29.
15. G. Fribourg, A. Deschamps, Y. Bréchet, and J.L. Chemin: *Proc. ICAA11*, J. Hirsch, B. Skrotzki, and G. Gottstein, eds., Wiley-VCH, Weinheim, Germany, 2008, pp. 936–46.
16. A. Deschamps, Y. Brechet, P. Guyot, and F. Livet: *Z. Metallkd.*, 1997, vol. 88, pp. 601–06.
17. M. Dumont, W. Lefebvre, B. Doisneau Cottignies, and A. Deschamps: *Acta Mater.*, 2005, vol. 53, pp. 2881–92.
18. A. Deschamps and F. de Geuser: *J. Appl. Cryst.*, 2011, vol. 44, pp. 343–52.